

## THERMOMECHANICAL-MICROSTRUCTURAL SIMULATION OF THE NODULAR CAST IRON SOLIDIFICATION PROCESS

Patricia M. Dardati<sup>a</sup>, Diego J. Celentano<sup>b</sup>, Fernando D. Carazo<sup>a</sup> and Luis A. Godoy<sup>c</sup>

<sup>a</sup>*Departamento de Ingeniería Mecánica y CIII, Facultad Regional Córdoba, UTN,  
Maestro M. López esq. Cruz Roja Argentina s/n, Ciudad Universitaria, Córdoba, Argentina,  
pdardati@industrial.frc.utn.edu.ar, <http://www.frc.utn.edu.ar>*

<sup>b</sup>*Departamento de Ingeniería Mecánica y Metalúrgica, Pontificia Universidad Católica de Chile, Av.  
Vicuña Mackenna 4860, Santiago, Chile, dcelentano@ing.puc.cl, <http://www.ing.puc.cl/icm>*

<sup>c</sup>*Departamento Estructuras, FCEFyN, Universidad Nacional de Córdoba y CONICET,  
Av. Vélez Sarsfield 1601, Córdoba, Argentina, lgodoy@com.uncor.edu, <http://www.efn.unc.edu>*

**Keywords:** nodular cast iron, solidification, microstructure, numerical simulation.

**Abstract.** This paper presents a thermomechanical-microstructural formulation for the analysis of the solidification process of nodular cast irons of eutectic composition. This formulation is defined in a finite strain thermoplasticity framework considering microstructure-based liquid-solid phase-change effects. The performance of this model is evaluated in the analysis of a solidification test, for which laboratory measurements are compared with the corresponding numerical results.

## 1 INTRODUCTION

The numerical simulation of the nodular (or spheroidal-graphite, S.G.) cast iron solidification and the subsequent cooling processes is still nowadays an active research area, mainly due to the different and complex phenomena involved in the analysis. Among the several factors that directly affect the final soundness of the castings, it is possible to identify the microstructure evolution, the presence of residual stresses, and the geometrical changes caused by thermal contraction and metallurgical transformations.

Several thermomechanical models, aimed at predicting thermal residual stresses and final shapes in castings in order to prevent macroscopic defects and/or to optimize operational conditions, have been developed during the last two decades; see e.g. [Celentano et al. \(1999\)](#) and references therein. On the other hand, relevant efforts have been done to couple heat flow calculations performed at the macroscopic level to related microscopic phenomena such as phase appearance, morphology and grain size with the sake of determining the ultimate mechanical properties of the solidified product; see e.g. [Rappaz \(1989\)](#) and references therein. More recently, some of these microstructural concepts have been considered in thermomechanical simulations of solidification and cooling processes of different alloys where microscopic models of microstructure formation are coupled to macroscopic thermomechanical computations to assess the influence of the evolution of both micro and macro features on the full response of the materials involved in the casting system ([Celentano, 2001](#); [Celentano, 2002](#)). In this last context, in sharp contrast to purely thermomechanical models, phase-change effects are assumed to depend not only on temperature but also on temperature rate by means of other appropriate microscopic variables to simulate in a more realistic form the complex phenomena associated with the phase transformation. However, it should be noted that this phenomenological approach includes the definition of evolution laws for the phase-change variables assumed to govern the average microstructure formation occurring in a certain (preferably small) volume at the macroscopic level and, hence, precludes a microscopic scale modelling of the micromechanisms developed during the process which, with the present computer power, is in most cases an impossible task.

This work presents a thermomechanical-microstructural formulation for the analysis of the solidification process of nodular cast irons with eutectic composition. This formulation, defined within the thermoplasticity context ([Celentano, 2002](#)), includes large strains effects, phase-change volumetric deformations, temperature-dependent material properties and microstructure evolution governed by a multinodular-based eutectic solidification model ([Dardati et al., 2006](#)).

The thermomechanical formulation is presented in Section 2. Section 3 includes the elasto-plastic constitutive model assumed to describe the behaviour of all the materials involved in the casting system and, in particular, the liquid, mushy and solid phases that take place during the solidification and cooling of the alloy. Thermoplasticity theory has been chosen for the constitutive description of the whole casting system since little rate-sensitiveness is expected in the material response due to the rapid evolution of the solidification and cooling processes. Moreover, this assumption is additionally supported by the fact that very similar thermomechanical behaviours have been obtained by using plastic and viscoplastic (with a relatively large range of viscosity values) models in the numerical simulation of casting problems ([Celentano, 2002](#)). Furthermore, the microstructure model of the eutectic nodular cast iron is described in Section 4. The microstructure mechanisms encompass kinetic-based nucleation and growth laws for both the dendritic austenite and graphite nodules.

This thermomechanical-microstructural model is discretized and solved in the context of

the finite element method; see [Celentano \(2002\)](#) for further details. Finally, the analysis of a solidification test is performed in Section 5 with the aim of comparing some available experimental measurements with the numerical results obtained using this proposed formulation.

## 2 THERMOMECHANICAL FORMULATION

In a general thermomechanical context, the local governing equations describing the evolution of a process can be expressed by the continuity equation, the equation of motion, the energy balance and the dissipation inequality (all of them valid in  $\Omega \times \mathcal{I}$ , where  $\Omega$  is the spatial configuration of a body and  $\mathcal{I}$  denotes the time interval of interest with  $t \in \mathcal{I}$ ) respectively written in a Lagrangian description as:

$$\rho J = \rho_0 \quad (1)$$

$$\nabla \cdot \boldsymbol{\sigma} + \rho \mathbf{b}_f = \rho \ddot{\mathbf{u}} \quad (2)$$

$$-\rho c \dot{T} - \nabla \cdot \mathbf{q} + \rho r - T \boldsymbol{\beta} : \mathbf{d} + \rho r_{int} = 0 \quad (3)$$

$$-\mathbf{q} \cdot \nabla T + D_{int} \geq 0 \quad (4)$$

together with appropriate boundary and initial conditions and adequate constitutive relations for the Cauchy stress tensor  $\boldsymbol{\sigma}$  (which is symmetric for the non polar case adopted in this work), the tangent specific heat capacity  $c$ , the heat flux vector  $\mathbf{q}$ , the tangent conjugate of the thermal dilatation tensor  $\boldsymbol{\beta}$ , the specific internal heat source  $r_{int}$  and the internal dissipation  $D_{int}$ . In these equations,  $\nabla$  is the spatial gradient operator, the superposed dot indicates time derivative and the subscript  $0$  applied to a variable denotes its value at the initial configuration  $\Omega_0$ . Moreover,  $\rho$  is the density,  $\mathbf{u}$  is the displacement vector,  $J$  is the determinant of the deformation gradient tensor  $\mathbf{F}$  ( $\mathbf{F}^{-1} = \mathbf{1} - \nabla \times \mathbf{u}$ , with  $\mathbf{1}$  being the unity tensor),  $\mathbf{b}_f$  is the specific body force vector,  $T$  is the temperature,  $r$  is the specific heat source and  $\mathbf{d}$  is the rate-of-deformation tensor ( $\mathbf{d} = 1/2(\nabla \times \mathbf{v} + \mathbf{v} \times \nabla)$ , where  $\mathbf{v} = \dot{\mathbf{u}}$  is the velocity vector). In this framework, a specific Helmholtz free energy function  $\psi$ , assumed to describe the material behaviour during the thermomechanical process, can be defined in terms of some thermodynamic state variables chosen in this work as the Almansi strain tensor  $\mathbf{e}$  ( $\mathbf{e} = 1/2(\mathbf{1} - \mathbf{F}^{-T} \cdot \mathbf{F}^{-1})$ , where  $^T$  is the transpose symbol), the temperature and a set of  $n_{int}$  phenomenological internal variables  $\boldsymbol{\alpha}_k$  (usually governed by rate equations with  $k = 1, \dots, n_{int}$ ) accounting for the non-reversible effects ([Lubliner, 1990](#)). This free energy definition is only valid for small elastic strains and isotropic material response, both assumptions being normally accepted for metals and other materials. Invoking the Coleman's method, the following relationships are obtained:  $\boldsymbol{\sigma} = \rho \frac{\partial \psi}{\partial \mathbf{e}}$ ,  $\eta = -\frac{\partial \psi}{\partial T}$  is the specific entropy function,  $c = -T \frac{\partial^2 \psi}{\partial T^2}$ ,  $\boldsymbol{\beta} = -\rho \frac{\partial^2 \psi}{\partial \mathbf{e} \partial T} = -\frac{\partial \boldsymbol{\sigma}}{\partial T}$ ,  $r_{int} = -\frac{1}{\rho} \left( T \frac{\partial \mathbf{q}_k}{\partial T} - \mathbf{q}_k \right) * \frac{D \boldsymbol{\alpha}_k}{Dt}$  and  $D_{int} = \mathbf{q}_k * \frac{D \boldsymbol{\alpha}_k}{Dt}$  where  $\mathbf{q}_k = -\rho \frac{\partial \psi}{\partial \boldsymbol{\alpha}_k}$  are the conjugate variables of  $\boldsymbol{\alpha}_k$  and, according to the nature of each internal variable, the symbols  $*$  and  $D(\cdot)/Dt$  appearing in the previous expressions respectively indicate an appropriate multiplication and a time derivative satisfying

the principle of material frame-indifference (Lubliner, 1990; Simo, 1995). Furthermore, the heat flux vector at the spatial configuration is assumed to be given by the Fourier's law written as  $\mathbf{q} = -k\nabla T$  where  $k$  is the conductivity coefficient. Additionally, a more restrictive dissipative assumption than that stated in equation (4) reads:  $-\mathbf{q} \cdot \nabla T \geq 0$  and  $D_{int} \geq 0$ . The first condition is automatically fulfilled for  $k \geq 0$  while the second imposes restrictions over the constitutive model definition.

It is seen that the definitions of  $\psi = \psi(\mathbf{e}, \alpha_k, T)$  and  $D\alpha_k/Dt$  are crucial features of the formulation in order to derive the constitutive equations presented above. To this end, the following split is proposed (Celentano et al., 1999):  $n_{int} = n_{int}^p + n_{int}^{pc}$ , where  $n_{int}^p$  and  $n_{int}^{pc}$  refer to the number of internal variables related to plastic (non-reversible that may occur in every material of the casting system) and phase-change (only existing in the solidifying alloy) effects, respectively. Accordingly, this assumption leads to  $r_{int} = r_{int}^p + r_{int}^{pc}$  and  $D_{int} = D_{int}^p + D_{int}^{pc}$ . Details of the elasto-plastic and microstructure models are given below.

### 3 ELASTO-PLASTIC CONSTITUTIVE MODEL

In this work, the material behaviour in the mushy zone is assumed to be governed by a mixed rule that weights the responses of the liquid ( $l$ ) and solid ( $s$ ) phases according to their respective volumetric fractions  $f$ . Thus, any mixed variable can be defined as:

$$\chi|_{mx} = \sum_{cp=l,s} f_{cp} \chi|_{cp} = f_l \chi|_l + f_s \chi|_s \quad (5)$$

such that  $\sum_{cp=l,s} f_{cp} = f_l + f_s = 1$ .

The internal variables and their corresponding evolution equations are defined in this work within the associate rate-independent thermoplasticity theory context (Lubliner, 1990; Simo, 1995). A possible choice is given by the plastic Almansi strain tensor  $\mathbf{e}^p$  and the effective plastic deformation  $\bar{e}^p$  related to the isotropic strain hardening effect (i.e.,  $n_{int}^p = 2$  with  $\alpha_1 = \mathbf{e}^p$  and  $\alpha_2 = \bar{e}^p$ ). The evolution equations for such plastic variables are written as:

$$L_v(\mathbf{e}^p) = \dot{\lambda} \partial F / \partial \sigma \quad \dot{\bar{e}}^p = -\dot{\lambda} \partial F / \partial C \quad (6)$$

where  $L_v$  is the well-known Lie (frame-indifferent) derivative,  $\dot{\lambda}$  is the plastic consistency parameter computed according to classical concepts of the plasticity theory,  $C$  is the plastic isotropic hardening function and  $F = F(\boldsymbol{\sigma}, \bar{e}^p, T)$  is the yield function governing the plastic behaviour of the solid such that no plastic evolutions occur when  $F < 0$ . A Von Mises yield function is adopted:

$$F = \sqrt{3J_2} - C_y|_{mx} \quad (7)$$

where  $J_2$  is the second invariant of the deviatoric part of  $\boldsymbol{\sigma}$  ( $\boldsymbol{\sigma}_{eq} = \sqrt{3J_2}$  is the so-called equivalent or Von Mises stress) and the yield strength function  $C_y|_{cp}$  is adopted in this work as:

$$C_y|_{cp} = C_{y0}|_{cp} + C \quad (8)$$

with  $C_{y_0}|_{cp} = C_{y_0}|_{cp}(T)$  being the yield strength defining the initial material elastic bound. In general,  $C_{y_0}|_{cp}$  decreases with temperature and, hence, it accounts for the thermal softening phenomenon, which is an important effect to be considered in casting processes where materials undergoing large temperature variations are involved. For the liquid phase, in particular,  $C_{y_0}|_l = 0$  is assumed.

Assuming a stress-free initial state ( $\boldsymbol{\sigma}_0 = \mathbf{0}$ ), the following specific free energy function  $\psi = \psi|_{mx}$  is proposed such that  $\psi|_{cp} = \psi|_{cp}(\mathbf{e} - \mathbf{e}^p, \bar{e}^p, T)$  is expressed as (Celentano, 2001; Celentano, 2002):

$$\psi|_{cp} = \frac{1}{2\rho} (\mathbf{e} - \mathbf{e}^p - \mathbf{e}^{th}|_{cp} - \mathbf{e}^{pc}) : \mathbf{C}^s|_{cp} : (\mathbf{e} - \mathbf{e}^p - \mathbf{e}^{th}|_{cp} - \mathbf{e}^{pc}) + \frac{I}{(n^p|_{cp} + 1)\rho} A^p|_{cp} \bar{e}^p|_{cp} + c^s|_{cp} [(T - T_0) - T \ln(T / T_0)] - L^s f_{cp} - \eta_0 (T - T_0) + \psi_0|_{cp} \quad (9)$$

where  $\mathbf{C}^s|_{cp}$  is the secant isotropic elastic constitutive tensor,  $A^p|_{cp}$  and  $n^p|_{cp}$  are the parameters aimed at characterising the isotropic hardening behaviour of the material,  $c^s|_{cp}$  is the secant specific heat and  $L^s$  is the secant specific latent heat. It should be noted that the deviatoric response of the liquid phase is neglected by assuming a purely volumetric elastic constitutive tensor in this phase. Furthermore,  $\mathbf{e}^{th}|_{cp}$  and  $\mathbf{e}^{pc}$  are the thermal and phase-change Almansi strain tensors, respectively given by:

$$\mathbf{e}^{th}|_{cp} = \frac{1}{2} [1 - (1 - a_{th}|_{cp})^{2/3}] \mathbf{1} \quad (10)$$

$$\mathbf{e}^{pc} = \frac{1}{2} [1 - (1 - a_{pc})^{2/3}] (1 - a_{th})^{2/3} \mathbf{1} \quad (11)$$

where  $a_{th}|_{cp} = \alpha_{th}^s|_{cp} (T - T_{ref}) - \alpha_{th_0}^s|_{cp} (T_0 - T_{ref})$  with  $\alpha_{th}^s|_{cp}$  being the secant volumetric thermal dilatation coefficient and  $a_{pc} = \delta_{pc}^s f_{cp}$  with  $\delta_{pc}^s$  being the secant phase-change volumetric deformation.

As mentioned above, the proposed definition of  $\psi$  allows the derivation, including coupled thermoelastic, thermoplastic and phase-change effects, of all the constitutive equations and internal dissipation by means of the expressions given in Section 2; see Celentano (2001) and Celentano (2002).

#### 4 MICROSTRUCTURAL MODEL

The eutectic nodular cast iron microstructure model adopted in this work corresponds to that proposed by Dardati et al., (2006). In this model, the phase-change internal variables are the austenite and graphite volumetric fractions together with their respective grain/nodule density and radius (i.e.,  $n_{int}^{pc} = \delta$ ). Only a brief description of this model is presented below.

#### 4.1 Solid fraction

Figure 1.a shows a schematic representation of an equiaxial dendrite grain and spherical graphite nodules. The total grain radius  $R_T$  is computed at the instant of instantaneous nucleation. The radius  $R_g$  corresponds to a spherical surface at the tip of the main dendrites and grows during the solidification until it reaches the value  $R_T$ . Three spherical symmetric zones are identified in Figure 1.b in order to produce a simplified description of the solute concentration (Rappaz and Thévoz, 1987). Zone 1, defined as a sphere with radius  $R_n$ , shows the evolution of the solute contents in the solid phase and covers the volumetric fraction corresponding to the total solid volume of the grain. Zone 2 shows a uniform distribution of solute in the interdendritic liquid while Zone 3 exhibits a variation of solute concentration in the intergranular region. In this context, the solid fraction is written as:

$$f_s = f_\gamma + f_{gr} \quad (12)$$

where  $f_\gamma$  and  $f_{gr}$  are the austenite and graphite volumetric fraction respectively given by:

$$f_\gamma = \left( \frac{R_n}{R_T} \right)^3 - f_{gr}^{Z_1} \quad (13)$$

$$f_{gr} = \sum_{i=1}^3 f_{gr}^{Z_i} \quad (14)$$

such that the graphite volumetric fraction of graphite associated to zone  $Z_i$  is:

$$f_{gr}^{Z_i} = \frac{4}{3} \pi \sum_{j=1}^k N_{gr_j}^{Z_i} R_{gr_j}^{Z_i 3} \quad (15)$$

where  $N_{gr_j}^{Z_i}$  is the number of graphite nodules per unit volume of total grain of zone  $Z_i$  with radius  $R_{gr_j}^{Z_i}$ , the subscript  $j$  denotes the nodule group related to a specific nucleation time and  $k$  stands for the total number of nodule groups.

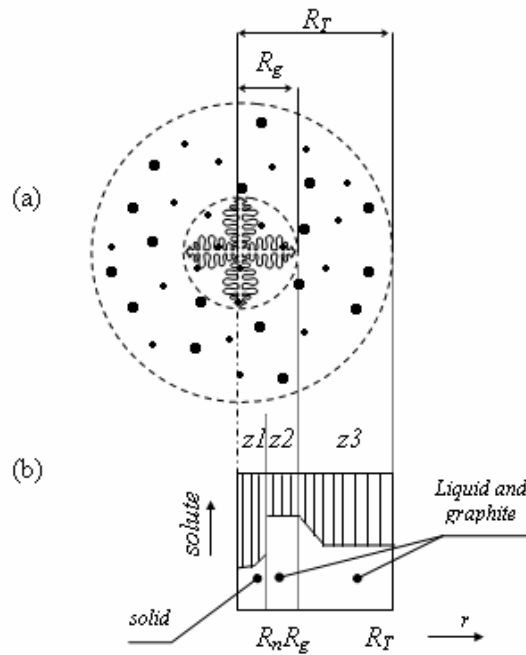


Figure 1: a) Schematic representation of an equiaxial dendrite grain and spherical graphite nodules, and b) spherical solute concentration (spherical symmetry is assumed).

#### 4.2 Nucleation and growth of austenite

Nucleation of the austenite is assumed to occur as soon as the eutectic temperature  $T_E$  is reached. The following instantaneous nucleation law is adopted:

$$N_\gamma = A_\gamma \dot{T} \tag{16}$$

where  $N_\gamma$  is the density of austenite grains and  $A_\gamma$  is a parameter that depends on the characteristics of liquid such as composition, superheating and holding time.

Based on the number of austenite grains that nucleate per unit volume, the total radius  $R_T$  is simply computed as:

$$R_T = \sqrt[3]{\frac{3}{4\pi N_\gamma}} \tag{17}$$

The growth of the dendrite tips is assumed to be controlled by the diffusion of solute while the influence of the thermal undercooling is neglected because the temperature is considered as constant for the whole grain. The evolution of  $R_g$  is given by:

$$\dot{R}_g = \frac{D_c^l m C_0}{\pi^2 \Gamma (k_p - 1)} \left( \frac{C^{l/\gamma} - C_\infty}{C_0} \right)^2 \tag{18}$$

where  $D_c^l$  is the coefficient of carbon diffusion in liquid,  $m$  is the slope of the austenite liquidus curve,  $C_0$  is the initial concentration of carbon,  $\Gamma$  is the Gibbs-Thompson coefficient,  $k_p$  is the partition coefficient,  $C^{l/\gamma}$  is the carbon concentration of the liquid in contact with austenite (at temperature  $T$  and at equilibrium) and  $C_\infty$  is the carbon

concentration of the intergranular liquid away from the dendrite tip.

Moreover, the radius of the spherical Zone 1 is evaluated by equating its volume to the sum of the eutectic austenite volume plus the volume of nodules that have already been surrounded by this phase and that do not continue growing according to this model. Thus,

$$\dot{R}_n = \frac{3R_g^2(C^{l/\gamma} - C_\infty)\dot{R}_g + (R_g^3 - R_n^3)\dot{C}^{l/\gamma}}{3C^{l/\gamma}(1 - k_p)R_n^2} \quad (19)$$

### 4.3 Nucleation and growth of graphite

Graphite nucleation is modeled as a continuous process that occurs in Zones 2 and 3 according to the following law:

$$\dot{N}_{gr_j}^{Z_i} = b_{gr} \Delta T \exp\left(-\frac{c_{gr}}{\Delta T}\right) (1 - f_s^{Z_i}) \quad (20)$$

where  $b_{gr}$  and  $c_{gr}$  are nucleation parameters that depend on the composition and liquid treatment and  $\Delta T$  is the undercooling.

Graphite nodules grow in both the interdendritic and intergranular liquids, but with different rates because Zones 2 and 3 have different carbon concentrations, named  $C^{l/\gamma}$  and  $C_\infty$ , respectively. The growth of graphite nodules due to diffusion is modeled here using Zener's equation for a spherical isolated particle in a matrix with low saturation:

$$\begin{aligned} \dot{R}_{gr_j}^{Z_2} &= \frac{D_c^l \rho_l (C^{l/\gamma} - C^{l/gr})}{R_{gr_j} \rho_{gr} (C_{gr} - C^{l/gr})} \\ \dot{R}_{gr_j}^{Z_3} &= \frac{D_c^l \rho_l (C_\infty - C^{l/gr})}{R_{gr_j} \rho_{gr} (C_{gr} - C^{l/gr})} \end{aligned} \quad (21)$$

where  $C^{l/gr}$  is the carbon concentration of the liquid in contact with graphite (at temperature  $T$  and at equilibrium) and  $C_{gr}$  is the carbon concentration of graphite (i.e., 100%).

## 5 SOLIDIFICATION TEST

The analysis of a cylindrical casting specimen of S.G. cast iron (diameter=70mm and height=140mm) in a green sand mould surrounded by a steel shell (internal diameter=185mm, thickness=30mm and height=260mm) is performed. This problem has been extensively studied using simplified infinitesimal strains constitutive models for the materials involved (Celentano et al., 1995; Celentano, 1997) and, more recently, involved large strains and microstructural effects (Celentano, 2001). The experimental apparatus is schematically shown in Figure 2. Both temperature and radial displacement evolutions have been measured during solidification and cooling approximately at the midheight of the specimen (Celentano, 2001). Thermocouples were placed on three radial directions at 0°, 120° and 240°, starting from the cylinder central axis to the surrounding sand mould in order to visualize the thermal gradient evolution. Radial displacements were measured at the same directions on the cylinder external skin using silica rods.

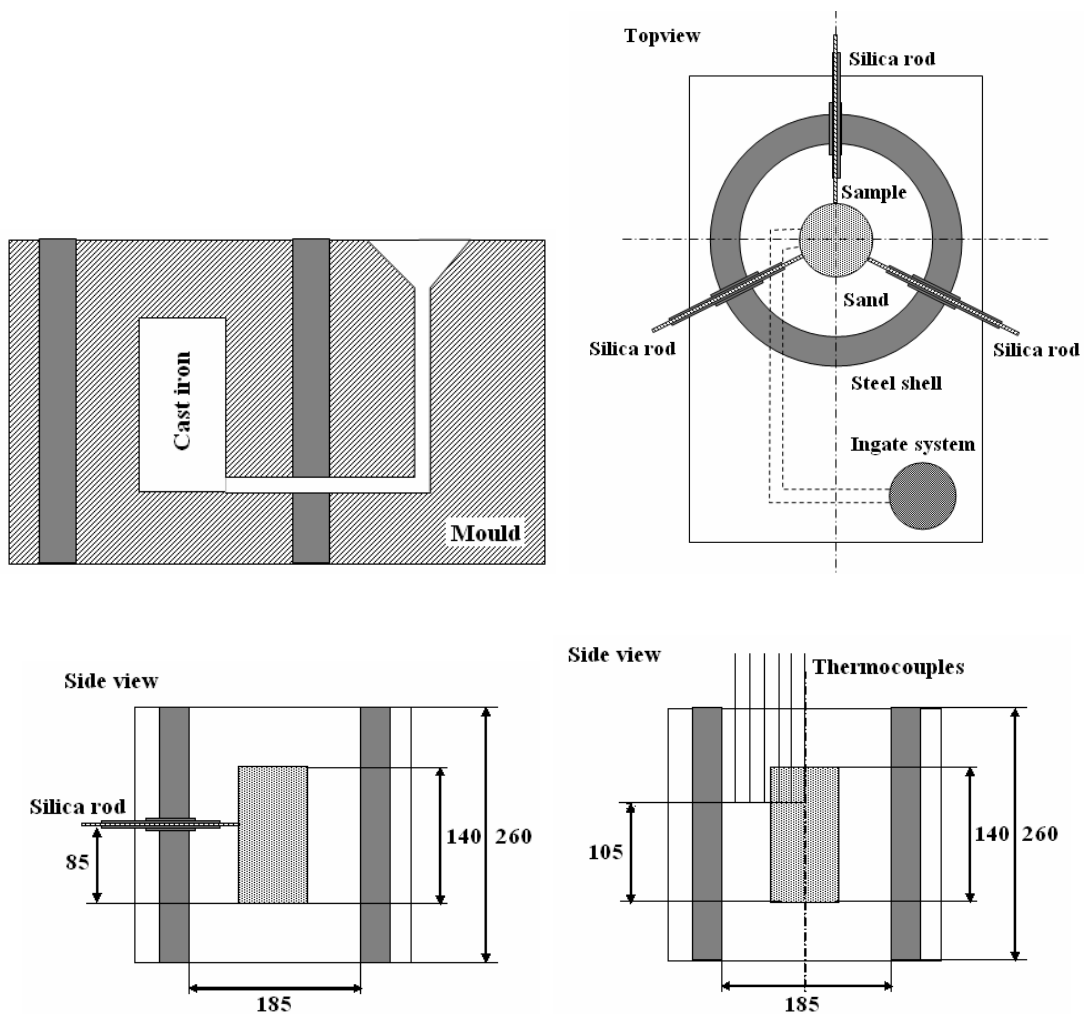


Figure 2: Experimental apparatus.

The material thermomechanical properties for the S.G. cast iron and green sand can be respectively found in [Celentano \(2001\)](#) and [Midea and Shah \(2002\)](#). The constants involved in the microstructural model for the S.G. cast iron are those reported in [Dardati et al. \(2006\)](#).

The axisymmetric numerical computation used 540 four-noded isoparametric elements and a time step of 50 s. The analysis starts with the mould cavity completely filled with molten metal at rest at 1250 °C (i.e., instantaneous filling is assumed) and 22 °C for the sand and steel moulds. The mould is simply supported at the bottom and convection-radiation conditions have been considered between the external face of the mould and the environment. The boundary conditions and the finite element mesh used are plotted in Figure 3. Mechanical frictionless contact conditions are adopted for the casting-sand interface.

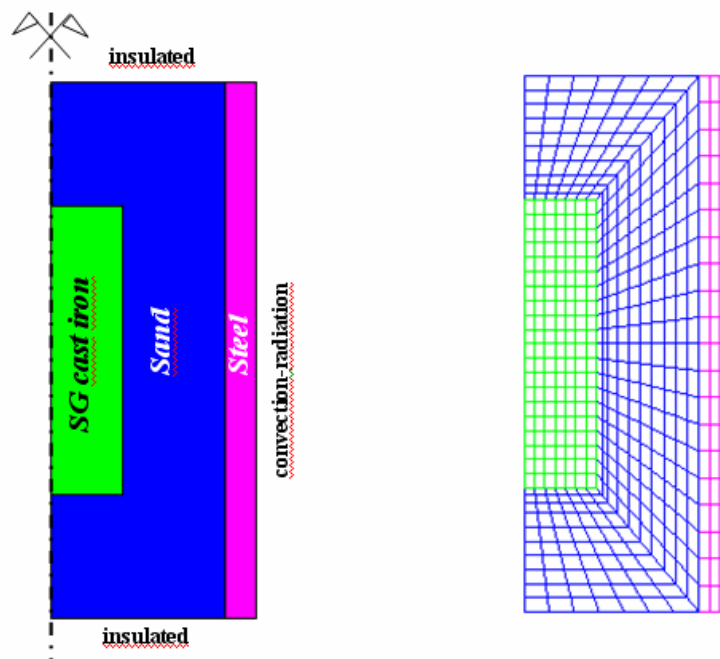


Figure 3: Boundary conditions and finite element mesh.

The experimental temperature evolutions in the casting for different radial positions at height 105 mm are plotted in Figure 4. The numerical results obtained with the proposed formulation are also included for comparison. A good overall agreement can be observed where, more specifically, the liquid-solid and solid-solid phase-changes are reasonably well described.

Experimental and computed temperature evolutions in the sand for different radial positions at height 105 mm are plotted in Figure 5 where, once again, a good fitting can be appreciated.

Moreover, the experimental and numerical radial displacement evolutions at height 85 mm of the casting-mould interface are shown in Figure 6. The different expansion/contraction behaviours related to the phase-changes occurring during the process can clearly be seen: a) contraction till the beginning of the solidification, b) expansion during solidification (graphite precipitation), c) contraction from the end of the solidification up to the beginning of the eutectoid transformation, d) contraction arrest during the eutectoid transformation and e) final contraction to room temperature. Almost identical behaviours have been experimentally observed for the three directions mentioned above and, therefore, an average curve has been included in Figure 6. Although the numerical fitting is only qualitative, the response provided by the S.G. model proposed in this work correctly reproduces the distinct behaviours observed at different stages of the process.

Figure 7 depicts the deformed configurations at four times of the analysis. It is seen that the differential vertical dilatation between the casting and sand mould that develops during the cooling process makes the measurement tasks difficult since the silica rods can be potentially broken as a consequence of the action of an unacceptable shear force.

The volumetric fractions evolutions in the casting for two radial distances at height 105 mm of the specimen are plotted in Figures 8 and 9. It is seen that the final graphite content is nearly independent of the temperature rate.

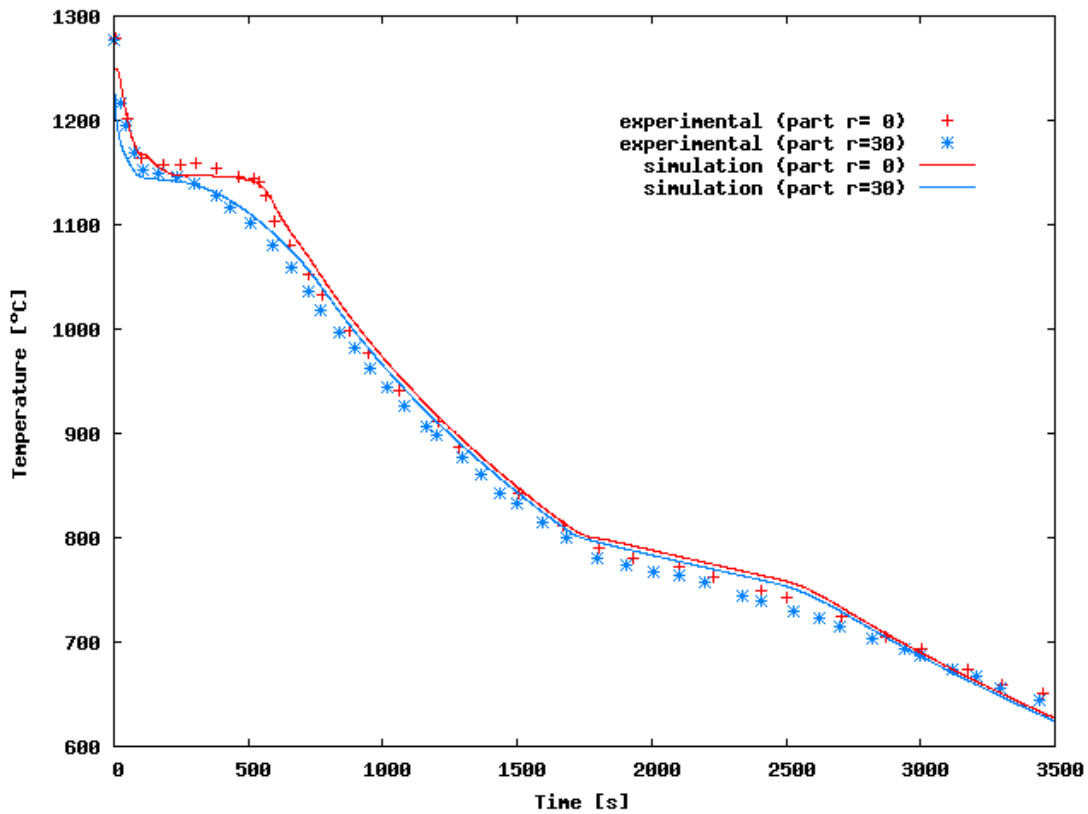


Figure 4: Temperature evolutions in the casting for different radial positions at height 105 mm of the specimen.

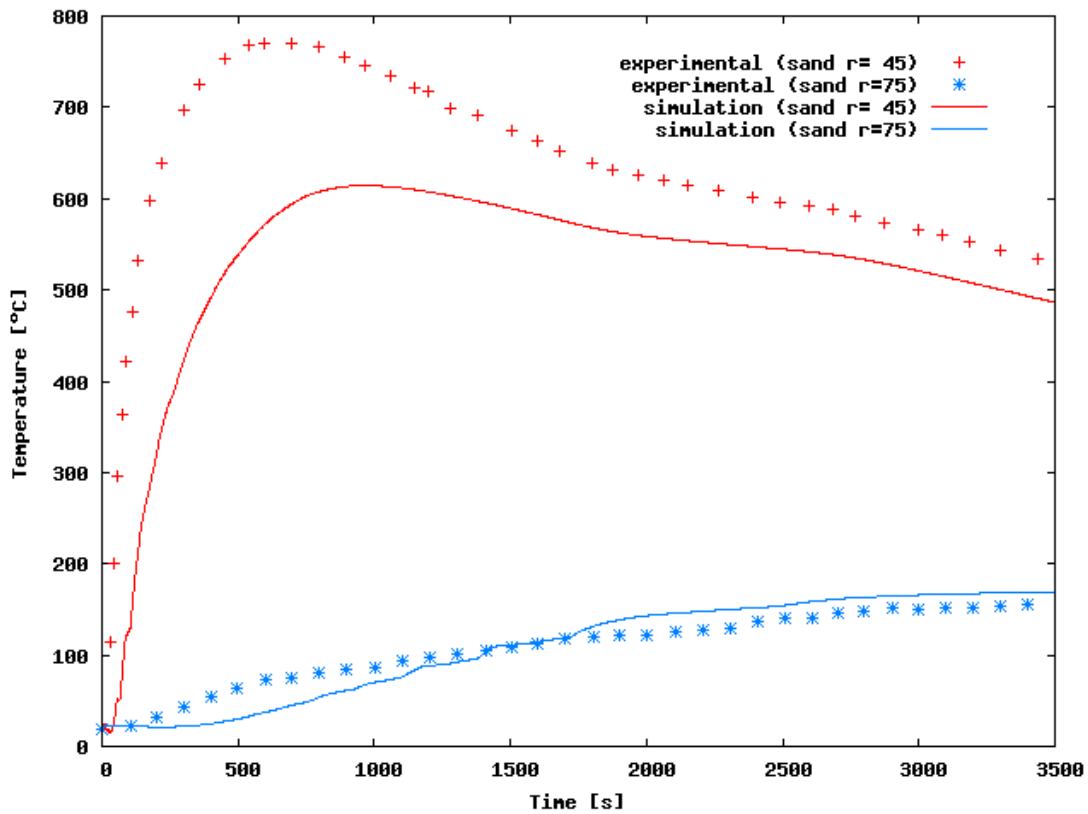


Figure 5: Temperature evolutions in the sand for different radial positions at height 105 mm of the specimen.

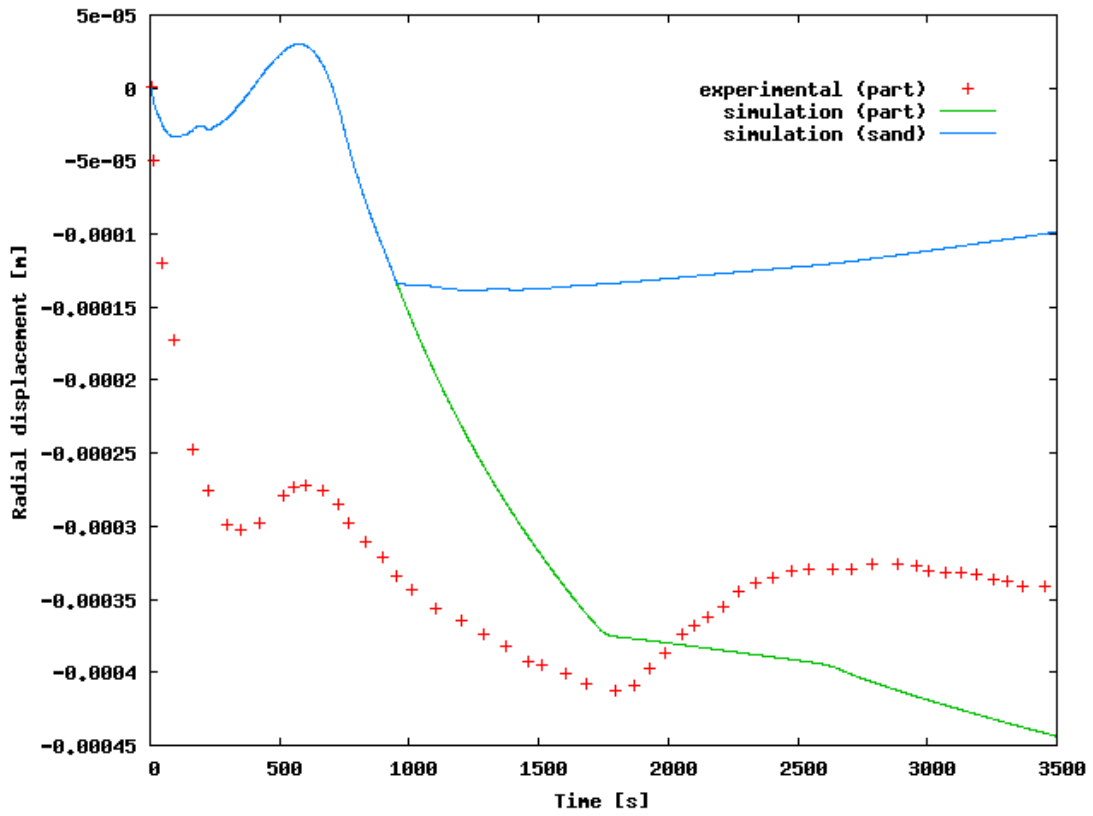


Figure 6: Radial displacement evolutions at height 85 mm of the casting-sand interface.

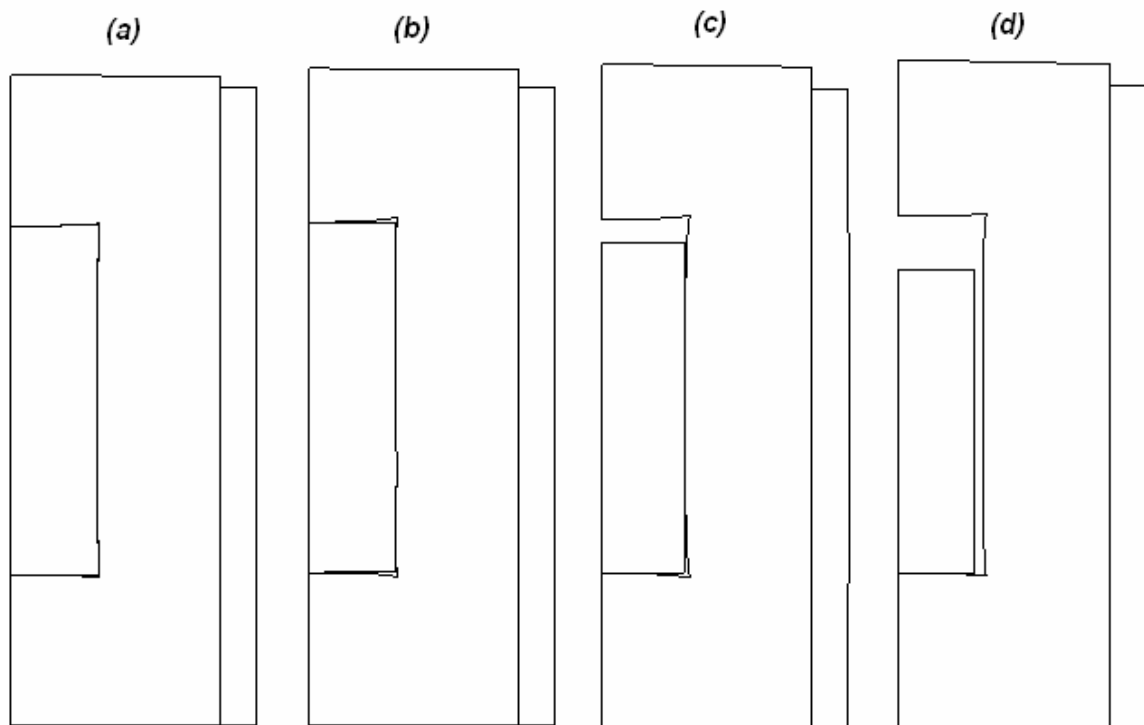


Figure 7: Deformed configurations at times a) 200 s, b) 500 s, c) 1000 s and d) 3500 s (amplification factor=10).

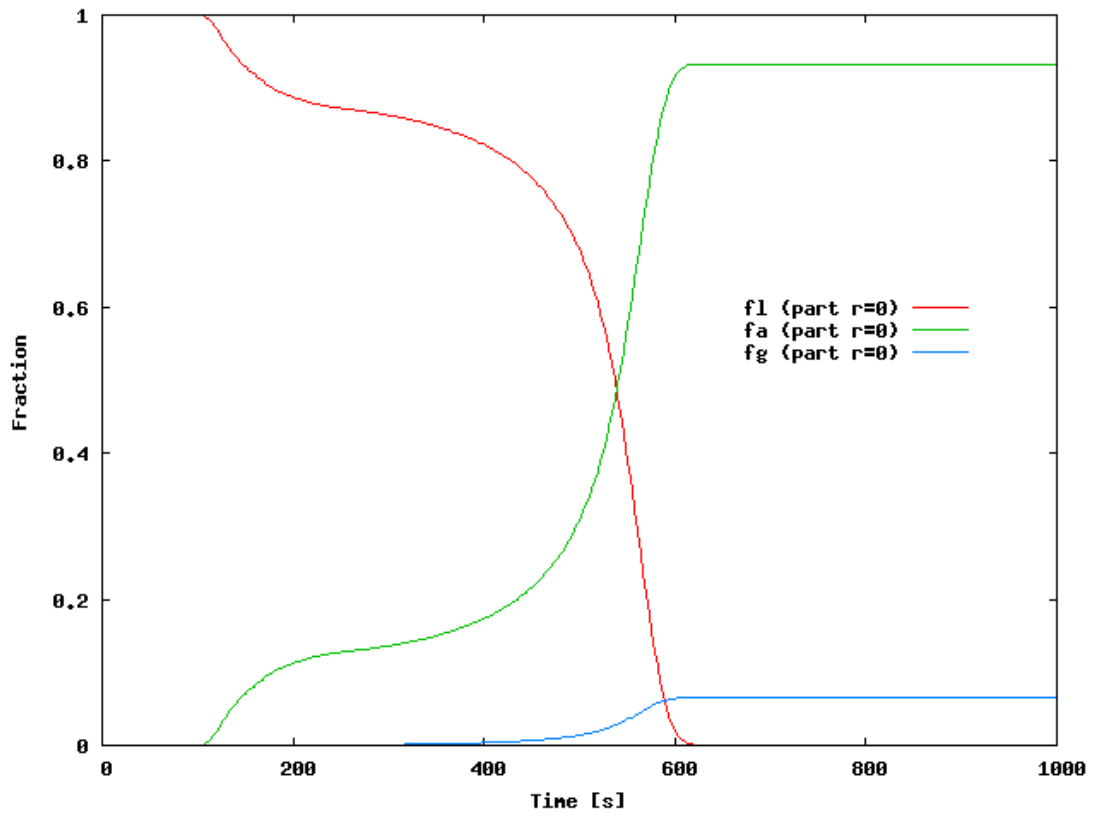


Figure 8: Volumetric fractions evolutions in the casting for radius 0 mm at height 105 mm of the specimen.

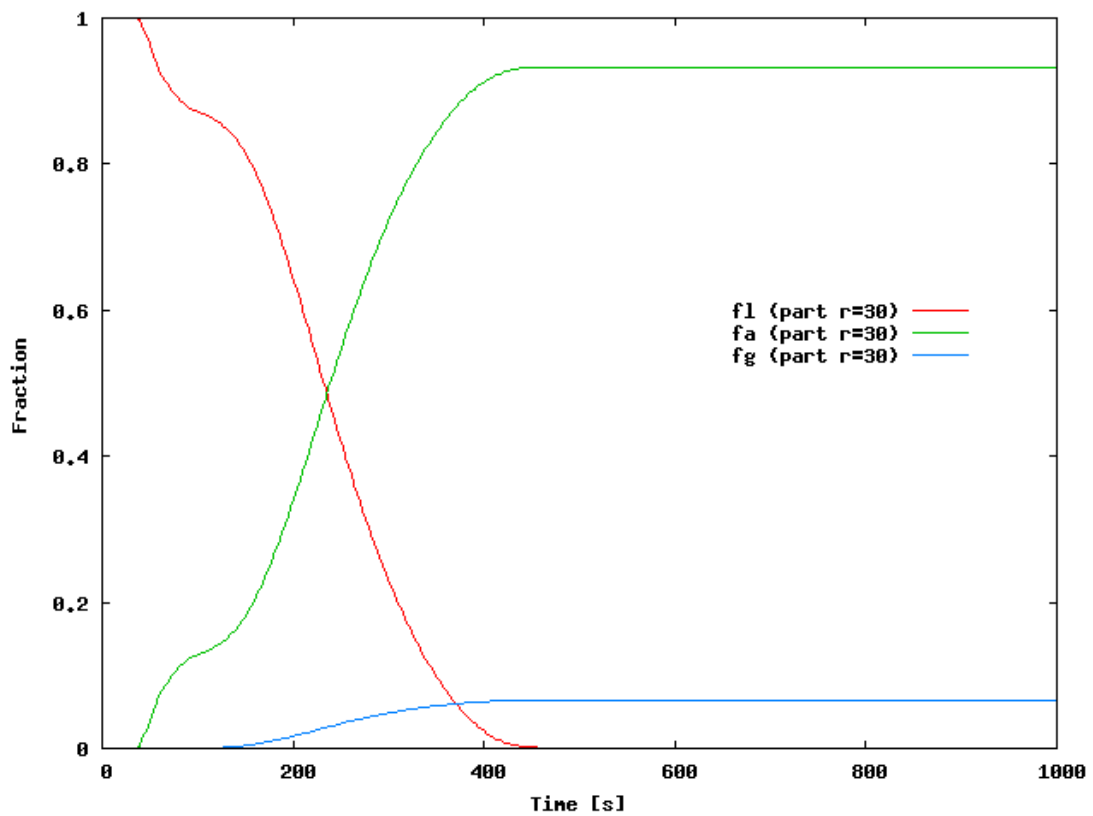


Figure 9: Volumetric fractions evolutions in the casting for radius 30 mm at height 105 mm of the specimen.

## 6 CONCLUSIONS

A large strain thermoplastic formulation for the analysis of the solidification process of nodular cast irons of eutectic composition has been presented. This formulation accounts for thermomechanical as well as microstructural behaviours of these materials in a unified framework allowing, therefore, to analyze the different coupled phenomena occurring in complex casting problems.

This formulation has been used in the analysis of a solidification test of nodular cast iron in a green sand mould. The model has been partially validated with some available experimental measurements where reasonable agreement between numerical and experimental results can be observed. However, the difficulties associated to the full material characterization lead to a further research in the thermomechanical/microstructural simulation of solidification processes with the sake of constituting a robust tool for casting design.

## 7 ACKNOWLEDGEMENTS

The support provided by CONICYT (FONDECYT Project N° 1060139) is gratefully acknowledged.

## REFERENCES

- Celentano, D., Visconte, D., Dardati, P., Oller S. and Oñate, E., A thermomechanical model for solidification problems: experimental validation. *Proceedings of COMPLAS IV*, R. Owen, E. Oñate and E. Hinton (Eds.), Pineridge Press/CIMNE, Swansea, U.K., 2385-2396, 1995.
- Celentano, D., A thermomechanical formulation for the solidification process of S.G. cast iron in a green sand mould. *Proceedings of COMPLAS V*, R. Owen, E. Oñate and E. Hinton (Eds.), Pineridge Press/CIMNE, Swansea, U.K., 1284-1288, 1997.
- Celentano, D., Gunasegaram, D., and Nguyen, T., A thermomechanical model for the analysis of light alloy solidification in a composite mould. *International Journal of Solids and Structures*, 36:2341-2378, 1999.
- Celentano, D., A large strain thermoviscoplastic formulation for the solidification of S.G. cast iron in a green sand mould. *International Journal of Plasticity*, 17:1623-1658, 2001.
- Celentano, D., A thermomechanical model with microstructure evolution for aluminium alloy casting processes. *International Journal of Plasticity*, 18:1291-1335, 2002.
- Dardati, P., Godoy, L. and Celentano, D., Microstructural simulation of solidification process of spheroidal-graphite cast iron. *ASME Journal of Applied Mechanics*, 73(6):977-983, 2006.
- Lubliner, J., *Plasticity Theory*. Macmillan Publishing, 1990.
- Midea, T. and Shah, J., Mold material thermophysical data. *AFS Transactions*, 02-080:1-16, 2002.
- Rappaz, M. and Thévoz, Ph., Solute diffusion model for equiaxed dendritic growth. *Acta Metallurgica*, 35:1487-1497, 1987.
- Rappaz, M., Modelling of microstructure formation in solidification processes. *International Materials Reviews*, 34:93-123, 1989.
- Simo, J., *Topics on the Numerical Analysis and Simulation of Plasticity*. Handbook of Numerical Analysis, Vol. III, Elsevier Science Publishers, 1995.